Available online at www.eccomasproceedia.org
Eccomas Proceedia COMPDYN (2023) 3842-3855

ECCOMAS
Proceedia

COMPDYN 2023
9th ECCOMAS Thematic Conference on
Computational Methods in Structural Dynamics and Earthquake Engineering
M. Papadrakakis, M. Fragiadakis (eds.)
Athens, Greece, 12-14 June 2023

A DAMAGE DETECTION APPROACH TO ASSESS THE PERFORMANCE LEVEL OF R/C BRIDGES USING VIBRATIONAL RESPONSE MEASUREMENTS

K. Mixios[1], O. Markogiannaki[2], S. Stefanidou[1], V. Papanikolaou[1]

[1] Aristotle University of Thessaloniki
Thessaloniki, Greece
e-mail: {mixioske, ssotiria, billy}@civil.auth.gr

[2] REDI Engineering Solutions PC
markogiannaki.olga@gmail.com

Abstract

Bridge damage presents risks to road safety and traffic flow, potentially resulting in significant economic losses, both direct and indirect. Therefore, there is an urgent need to develop and implement systems for evaluating the structural health of bridges. This study introduces a methodology that utilizes measured vibration data from initial and damaged responses of a monitored bridge system to identify damage. A highly detailed finite element model consistent with the measured data is employed for this purpose. The model parameters of the damaged structure are estimated using optimization algorithms to identify, localize, and quantify damage. Capacity curves for both the calibrated and the damaged bridge are developed to evaluate the effect of the damage on the global response of the bridge. The approach is applied to monolithic R/C bridge in a case study, and simulated experiments (e.g. damage scenarios) are conducted to demonstrate the proposed methodology.

Keywords: capacity curves, damage detection, R/C bridges.

ISSN:2623-3347
Peer-review under responsibility of the organizing committee of COMPDYN 2023.
doi: 10.7712/120123.10684.22588

1 INTRODUCTION

The research topic of identifying structural damage in bridges has gained significant attention over the years. Its increased popularity can be primarily attributed to the aging road and rail infrastructure, which faces traffic loading conditions that far exceed the original design criteria. This unprecedented increase in loading speeds up structural fatigue, leading to a decrease in the service life of these bridges. Moreover, as the bridge infrastructure continues to age and deteriorate, it becomes necessary to increase the frequency of inspections to compensate for the reduced safety of these structures. However, this task is challenging due to its immense scale. Europe has approximately one million highway bridges, and 35% of its half a million rail bridges are over a century old [1]. Consequently, there has been a significant surge in research focused on effectively managing the maintenance and upkeep of these bridges [2]. One area of study that has gained prominence is the investigation of vibration-based techniques for detecting and identifying damage.

In the past few decades, the most extensively studied techniques for detecting damage in structures have been traditional modal-based methods. The concept of utilizing measured vibrations to identify structural damage has been employed for quite some time. Traditional modal parameters such as shifts in natural frequency and other modal properties like mode shapes, damping ratios, and modal curvatures have conventionally been utilized for damage detection [3]. Ideally, these properties should be obtained dynamically from a bridge prior to its initial opening, if feasible, using ambient and forced vibration. Mode shapes offer distinct advantages as they are less affected by environmental factors compared to natural frequencies. Additionally, they encompass both local and global information, making them valuable for damage localization. Over the years, several mode shape monitoring techniques have been developed. One such technique is the modal assurance criterion (MAC) [4], [5], which assesses changes in mode shapes across the entire structure by utilizing eigenvector orthogonality. Building upon MAC, Kim et al [6] introduced the coordinate modal assurance criterion (CO-MAC), which monitors modal node displacement to detect and pinpoint damage. COMAC can be applied to a node i by measuring the normalized difference between mode shape vectors under undamaged ($\varphi u_{i,j}$) and damaged ($\varphi d_{i,j}$) conditions. The application of MAC and COMAC in bridge structures revealed that these methods not only detected most structural changes and their locations but also identified instances of false or spurious damage [7]. Nevertheless, modal-based methods encounter limitations in terms of efficiency when local damage does not significantly alter the modal properties of the structure. This is particularly true when the severity of the damage has a minimal impact on the overall integrity of the structural system. As a result, damage indicators that rely on measured data directly come into play, encompassing various approaches such as frequency response functions (FRFs), operating deflection shapes, and transmittance functions, among others [8]. To address the limitations of conventional structural damage detection methods, various frameworks for structural monitoring have been developed, as highlighted by [8], [9].

This study introduces a novel framework for damage detection in reinforced concrete (R/C) bridges, focusing on the utilization of vibrational measurements and on the estimation of the severity of the identified damage. The computational framework employs the Dynamic Mode Decomposition method to detect potential damages in R/C bridges, and the results are validated using a reference finite element model with selected damage scenarios. The location and severity of the identified damage are determined through a model update process utilizing the Particle Swarm Optimization algorithm. Furthermore, the proposed approach involves comparing the capacity curves of the models towards an accurate estimation of the severity of the damage in relation to the bridge system. The framework is applied to a typical three-span

bridge, utilizing simulated acceleration recordings for the chosen damage scenarios. The results demonstrate the reliability of the proposed process, providing valuable information about the actual condition of the bridge to stakeholders.

2 METHODOLOGY

This research paper presents a detailed approach to identifying damage in reinforced concrete (R/C) bridges. The methodology places significant emphasis on localizing and quantifying the extent of damage within bridge components by utilizing vibrational measurements. The following outlines the specific stages of the methodology:

Step 1: A finite element model of the structure studied is created using appropriate finite element software (e.g., OpenSees [10]). Ensuring the simulation's accuracy with respect to the physical model is crucial for more precise damage calculations. The model of step 1 is the healthy model of the considered structure.

Step 2: A sensitivity analysis is conducted. The purpose of conducting a sensitivity analysis is to identify the crucial parameters in a model. This analysis helps in clustering the parameters of the bridge model, such as Young's modulus of elasticity and moment-curvature relationships of pier sections, based on the similarity of their effects on the model's response. The sensitivity analysis in this case utilizes the mode shapes as the objective function. Another commonly employed method in such applications is the frequency response function (FRF) [8].

Step 3: The capacity curve of the healthy bridge is estimated via pushover analysis of the bridge system [11]. To conduct the pushover analysis, a horizontal load is applied longitudinally along the bridge's span, specifically at the locations corresponding to the piers. This load distribution enables the evaluation of the structural response and performance under progressively increasing displacement demands, providing valuable insights into the behavior of the bridge.

Step 4: The development of damaged models involves considering various damage scenarios based on the reference model. Once the model parameters have been clustered, modified values are assigned to the variables within the most sensitive clusters to create the damaged models. The number of variables can vary depending on the complexity of the model simulation. In accordance with the structural bridge system, different damage scenarios are chosen for analysis.

Step 5: The damaged bridge response is measured by determining the locations for placing accelerometers on the bridge deck. These accelerometers are positioned at locations where a series of maximum eigen-displacements are expected to occur. One advantage of having a finite element model before conducting field investigations is that it provides valuable insights into the behavior of the structure. Installing multiple accelerometers can improve the accuracy of the results, as it allows for a more precise observation of the system's response. In on-site applications, it is recommended to attach the accelerometers to the center of the bridge deck to avoid any torsional effects.

Step 6: Damage detection using Dynamic Mode Decomposition (DMD) [12]. The acceleration data retrieved from the sensors are used in the procedure of Dynamic Mode Decomposition (DMD). DMD is data-driven by nature, and the first step is to collect snapshots pairs of a system's state as it develops over time. These snapshot pairings are designated as $\{(x(t_k), x(t'_k))\}_{k=1}^{m}$, where $t'_k = t_k + \Delta t$ and the time-step Δt in order to identify high frequencies A snapshot represents the state of a system, reshaped into a high-dimensional column vector. These snapshots can be depicted in two data matrices $\boldsymbol{X}, \boldsymbol{X'}$.

$$\boldsymbol{X} = [\, x(t_1) \quad x(t_2) \ \ldots \quad x(t_m)] \tag{1}$$

$$\boldsymbol{X'} = [\, x(t'_1) \quad x(t'_2) \ \ldots \quad x(t'_m)] \tag{2}$$

The DMD algorithm seeks the leading spectral decomposition of the most accurate fitted linear operator **A** that correlates the two snapshot matrices in the time domain.

$$\boldsymbol{X'} \approx \boldsymbol{AX} \tag{3}$$

Operator **A** then establishes a linear dynamic system that best advances snapshot measurements in time. The best-fit operator A is defined as:

$$A = argmin\left|\left|\boldsymbol{X'} - \boldsymbol{AX}\right|\right|_F \tag{4}$$

An ambient vibration is imposed to retrieve the damaged model's state due to the basic assumption of DMD. DMD provides a modal decomposition consisting of spatially correlated components that have the same linear behavior in time. Therefore, the state of the bridge is not changing over time.

The DMD procedure is summarized in the following steps:

- The singular value decomposition of **X** is computed.

$$\boldsymbol{X} \approx \widetilde{\boldsymbol{U}}\widetilde{\boldsymbol{\Sigma}}\widetilde{\boldsymbol{V}}^* \tag{5}$$

Where $\widetilde{\mathbf{U}} \in \mathbb{C}^{n\times r}, \widetilde{\mathbf{\Sigma}} \in \mathbb{C}^{r\times r}$, and $\widetilde{\mathbf{V}} \in \mathbb{C}^{m\times r}$, and $r \leq m$ denotes either the exact or the approximate rank of the data matrix **X**.

- A full matrix A is obtained, computing the pseudo-inverse of **X**.

$$\mathbf{A} = \mathbf{X'}\widetilde{\mathbf{V}}\widetilde{\mathbf{\Sigma}}^{-1}\widetilde{\mathbf{U}}^* \tag{6}$$

- The spectral decomposition of **A** is computed:

$$\widetilde{\mathbf{A}}\mathbf{W} = \mathbf{W}\boldsymbol{\Lambda} \tag{7}$$

- The high-dimensional DMD modes $\boldsymbol{\Phi}$ are reconstructed using the eigenvectors **W** of the reduced system and the time-shifted snapshot matrix $\boldsymbol{X'}$ according to

$$\boldsymbol{\Phi} = \mathbf{X'}\widetilde{\mathbf{V}}\widetilde{\mathbf{\Sigma}}^{-1}\mathbf{W} \tag{8}$$

- Remarkably, these DMD modes are eigenvectors of the high-dimensional **A** matrix corresponding to the eigenvalues in $\boldsymbol{\Lambda}$.

$$\begin{aligned}\mathbf{A}\boldsymbol{\Phi} &= \left(\mathbf{X'}\widetilde{\mathbf{V}}\widetilde{\mathbf{\Sigma}}^{-1}\underbrace{\widetilde{\mathbf{U}}^*\big)\big(\mathbf{X'}\widetilde{\mathbf{V}}\widetilde{\mathbf{\Sigma}}^{-1}}_{\widetilde{\mathbf{A}}}\mathbf{W}\right)\\ &= \mathbf{X'}\widetilde{\mathbf{V}}\widetilde{\mathbf{\Sigma}}^{-1}\widetilde{\mathbf{A}}\mathbf{W}\\ &= \mathbf{X'}\widetilde{\mathbf{V}}\widetilde{\mathbf{\Sigma}}^{-1}\mathbf{W}\boldsymbol{\Lambda}\\ &= \boldsymbol{\Phi}\boldsymbol{\Lambda}.\end{aligned} \tag{9}$$

The state of the model is finally defined utilizing the eigenvectors calculated above. The localization of the damage is the output of a model update process. The methodology followed for the model update is based on particle swarm optimization (PSO) described in Fig. 1 as proposed in [13] and is described in detail below.

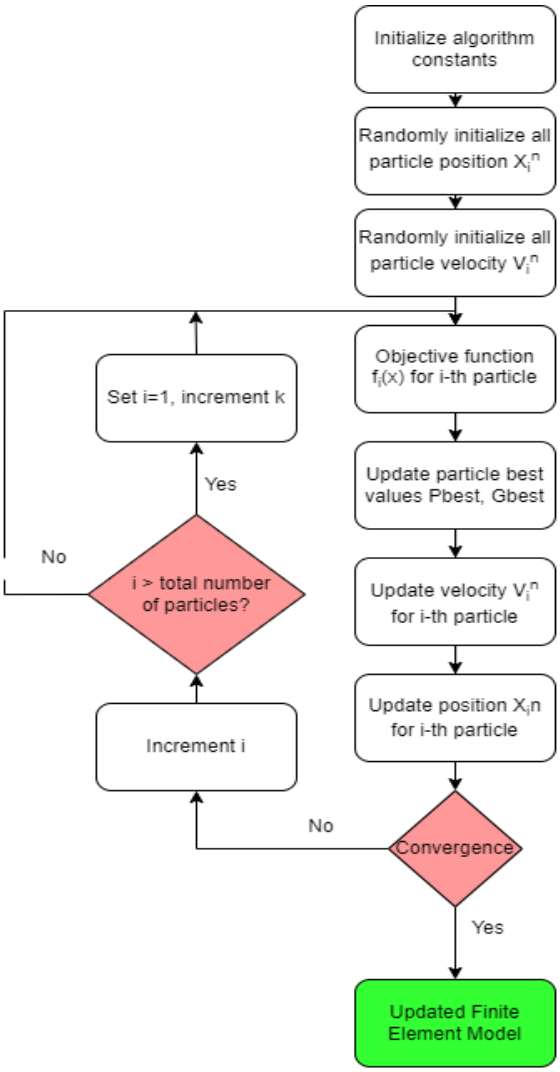

Figure 1. Workflow of the Particle Swarm Optimization procedure.

The main steps can be summarized as follows:

- Initialization of the algorithm constants (position and velocity vectors), definition of the number of particles. Definition of an objective function. Recording and updating the best particle position and the best position ever reached.
- Updating the velocity of each particle based on:

$$\boldsymbol{x}_{ij}^{n+1} = \boldsymbol{x}_{ij}^{n} + \boldsymbol{v}_{ij}^{n+1} \tag{10}$$

where v_{ij}^{n+1} is the velocity vector and x_{ij}^{n+1} is the position vector in the iteration n + 1, $\boldsymbol{x}_{ij}^{n}$ is the position vector in iteration n. The velocity vector of the particle swarm is calculated with the equation:

$$\boldsymbol{v}_{ij}^{n+1} = w\boldsymbol{v}_{ij}^{n} + C_1\text{rand}_1\left(\textbf{Pbest}_{ij} - \boldsymbol{x}_{ij}^{n}\right) + C_2\text{rand}_2\left(\textbf{Gbest}_{j} - \boldsymbol{x}_{ij}^{n}\right) \quad (11)$$

where C1 and C2 are the learning factors, and rand_1 and rand_2 the random values between 0 and 1. Pbest_{ij} and Gbest_{j} are the best positions that i-th particle achieved closest to the target since the start of the procedure.

- Update the position of every particle based on the behavior of the swarm.

The above method ends when the termination criteria are fulfilled. Fig. 1 depicts the particle swarm optimization method. PSO does not require any knowledge of the function formula or its derivatives and can investigate numerous potential solutions. Since it is a global approach, its performance is independent of the original population solutions.

Step7: Finally, a pushover analysis is performed on the updated model with damage in order to extract its capacity. The new capacity of the model is compared to the initial capacity of the model (healthy model) in terms of displacement ductility (δ_4/δ_y).

The workflow of the methodology proposed herein containing the steps described above is shown in Fig. 2.

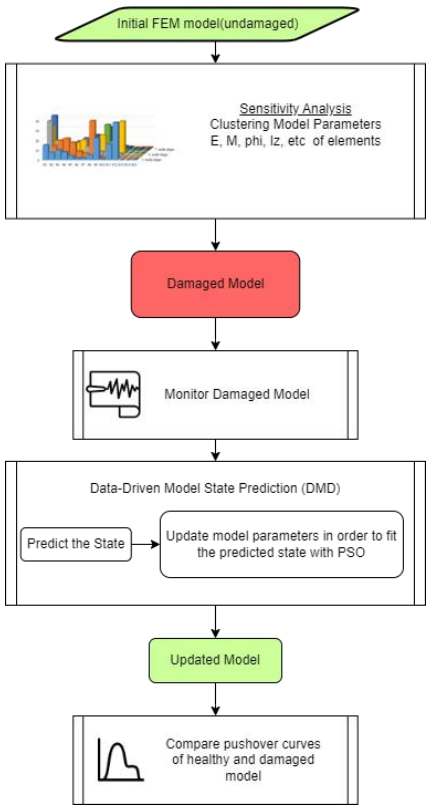

Figure 2. Workflow of the proposed methodology.

3 CASE STUDY

The described methodology is implemented on a typical three-span bridge located in Northern Greece. The bridge consists of three spans, with the outer spans measuring 27 m each and the central span measuring 45 m. The deck of the bridge is a prestressed concrete box girder section, 10 m wide. The piers have a solid circular reinforced concrete section with a diameter of 2.0 m and are connected monolithically to the deck. Figure 3 illustrates that the left pier has a height of 7.9 m, while the right pier has a height of 9.3 m due to the longitudinal slope of the bridge axis. The abutments of the bridge are seat-type, with a backwall height of 2.5 m [14], [15]. At the abutment positions, the deck is supported by two elastomeric bearings.

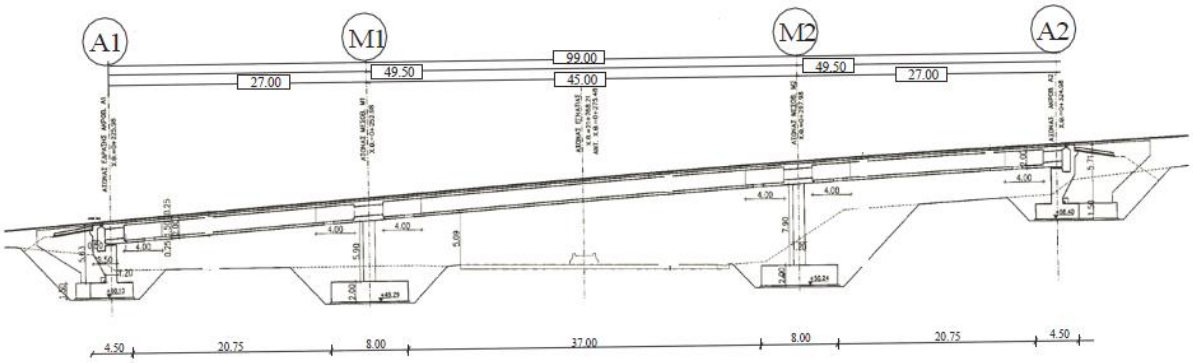

Figure 3. Longitudinal section of the bridge model.

Parameters		Lower Bound	Upper Bound	Nominal Values
Young Modulus E (right pier) [MPa]	1	18733.20	43710.80	31222.00
Young Modulus E (left pier) [kPa]	2	18733.20	43710.80	31222.00
Yielding Moment Top Section – My_top(left pier) [kNm]	3	16770.8	39131.9	27951.4
Yielding Moment – My_bottom (left pier) [kNm]	4	16883.0	39393.6	28138.3
Ultimate Moment Top Section – Mu_top(left pier) [kNm]	5	17185.8	40100.2	28643.0
Ultimate Moment Bottom Section – Mu_bottom (left pier) [kNm]	6	17280.7	40321.6	28801.2
Yielding Moment Top Section – Mu_top (right pier) [kNm]	7	16735.6	39049.8	27892.7

Yielding Moment Bottom Section – My_bottom (right pier) [kNm]	8	16895.3	39422.4	28158.9
Ultimate Moment Top Section – Mu_top (right pier) [kNm]	9	17153.22	40024.2	28588.7
Ultimate Moment Bottom Section – Mu_bottom	10	17287.1	40336.6	28811.9
Yielding curvature Top Section – curvature_top (left pier)	11	17287.1	40336.6	28811.9
Yielding curvature Bottom Section – curvature_bottom (left pier)	12	0.001706014	0.0039807	0.002843357
Ultimate curvature Top section – curvature_top (left pier)	13	0.00169238	0.00395789	0.002827064
Ultimate curvature Bottom section – curvature_bottom (left pier)	14	0.04416	0.10304	0.0736
Yielding curvature Top section – curvature_top (right pier)	15	0.001707499	0.003984163	0.002845831
Yielding curvature Bottom Section – curvature_bottom (right pier)	16	0.001695788	0.00395684	0.002826314
Ultimate curvature Top Section – curvature_top (right pier)	17	0.4416	0.10304	0.0736
Ultimate curvature Bottom Section – curvature_bottom (right pier)	18	0.04416	0.10304	0.0736
Gaps	19	0.01	0.10	0.10

Table 1. Parameters of cluster A grouped from the sensitivity analysis. Lower and Upper Bounds is also given for the sensitivity analysis.

The model was constructed using OpenSeesPy [16], which is a Python library serving as an interface to the OpenSees software. The bridge elements are modeled as elastic, while the piers incorporate a plastic hinge formulation at both ends. The applied loads on the bridge are limited to gravitational forces. To generate the damaged model, a sensitivity analysis and

clustering procedure were conducted. As mentioned earlier, the parameters were grouped based on their influence on the bridge's response, utilizing the unweighted multiple group method with arithmetic mean [17].

The results of the sensitivity analysis are summarized in Table 1. Two damage scenarios were executed to assess and validate the proposed methodology (Fig. 4). In the first scenario, a decrease in the yield moment and Young's modulus of elasticity was applied to the left pier. The same reduction was implemented for the right pier in the second scenario. Extended damage was represented by a 40% reduction in the properties of the pier elements. Furthermore, is assumed that the gaps between the deck and the abutments are effectively closed.

The locations for placing acceleration recorders on the bridge deck were determined based on where the maximum eigen displacements occur (Fig. 5). Modal analysis was performed on the reference model to obtain the eigenmodes and the model's response. To apply the proposed methodology, simulated damage scenarios were considered, and the Dynamic Mode Decomposition (DMD) process was implemented. Given the complexity of existing libraries, the authors developed a lightweight Python library for this purpose. The result of the DMD procedure is the state of the damaged model. Particle swarm optimization is employed to determine the values of the model parameters that correspond to the specific damage scenario being considered.

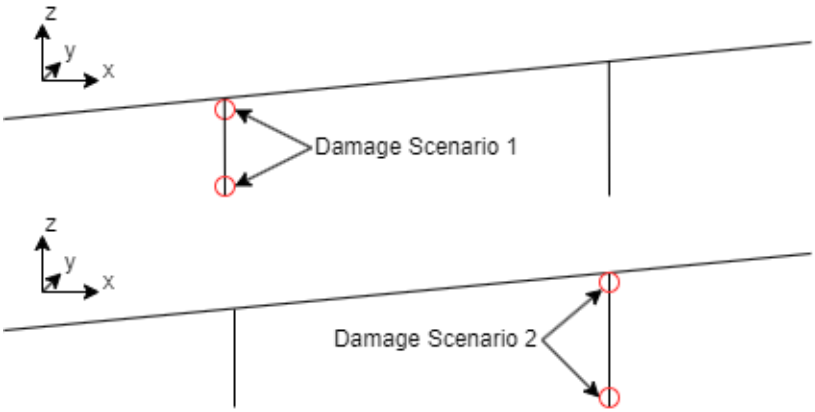

Figure 4. Locations of the damge scenarios implementation

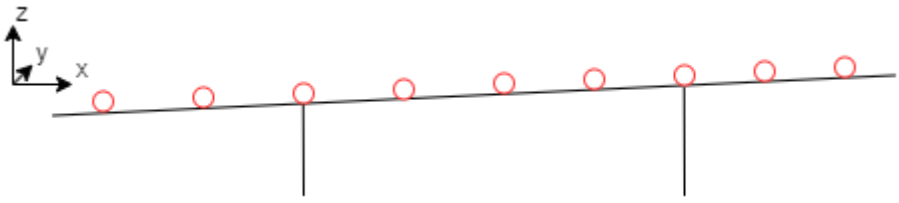

Figure 5. Acceleration recorder location on the bridge deck

4 RESULTS AND CONCLUSIONS

The efficiency of the proposed methodology is demonstrated in Figures 6-7. The predicted damaged model exhibits periods that are comparable to the initial model with damage in both scenarios. This indicates that the DMD process accurately captures the modal properties of the dynamic system. Figure 8 illustrates the changes in the model's behavior resulting from the damage scenarios in relation to the healthy model. The slight discrepancies can be attributed to the numerical assumptions and computational procedures of the solver used in the analysis. It is evident that these differences are marginal.

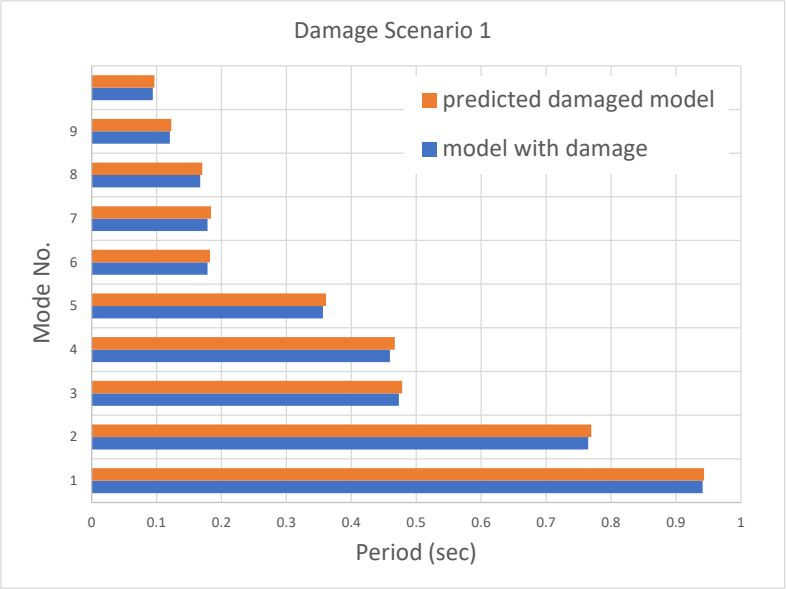

Figure 6. Comparison of the known damaged model and the predicted damaged model. (Scenario 1)

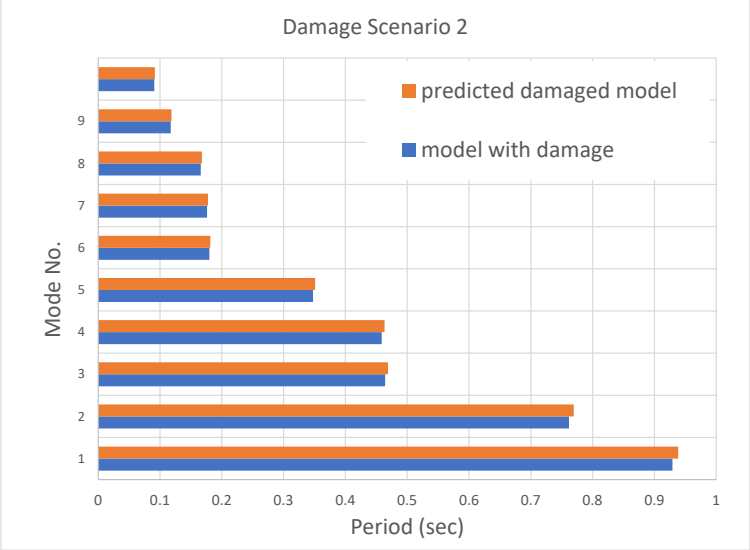

Figure 7. Comparison of the known model and the predicted damaged model. (Scenario 2)

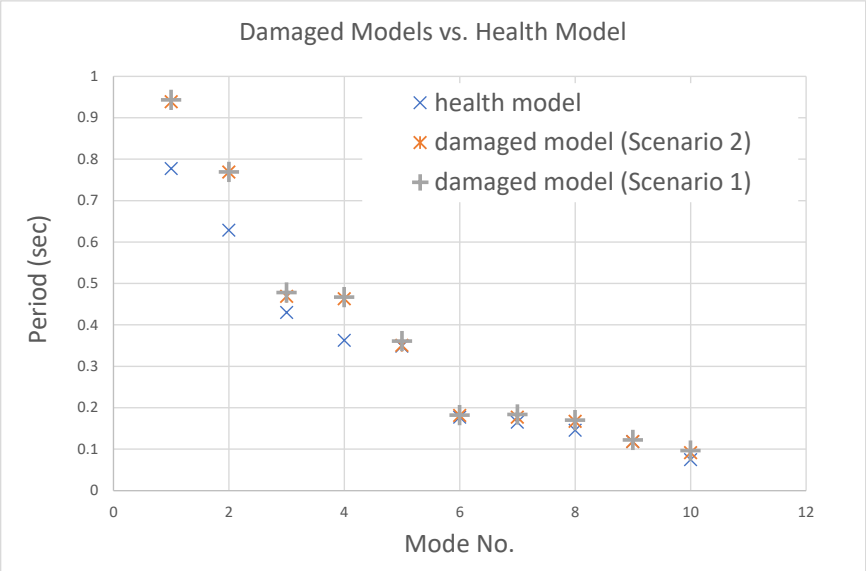

Figure 8. Comparison of Undamaged model and known damaged models.

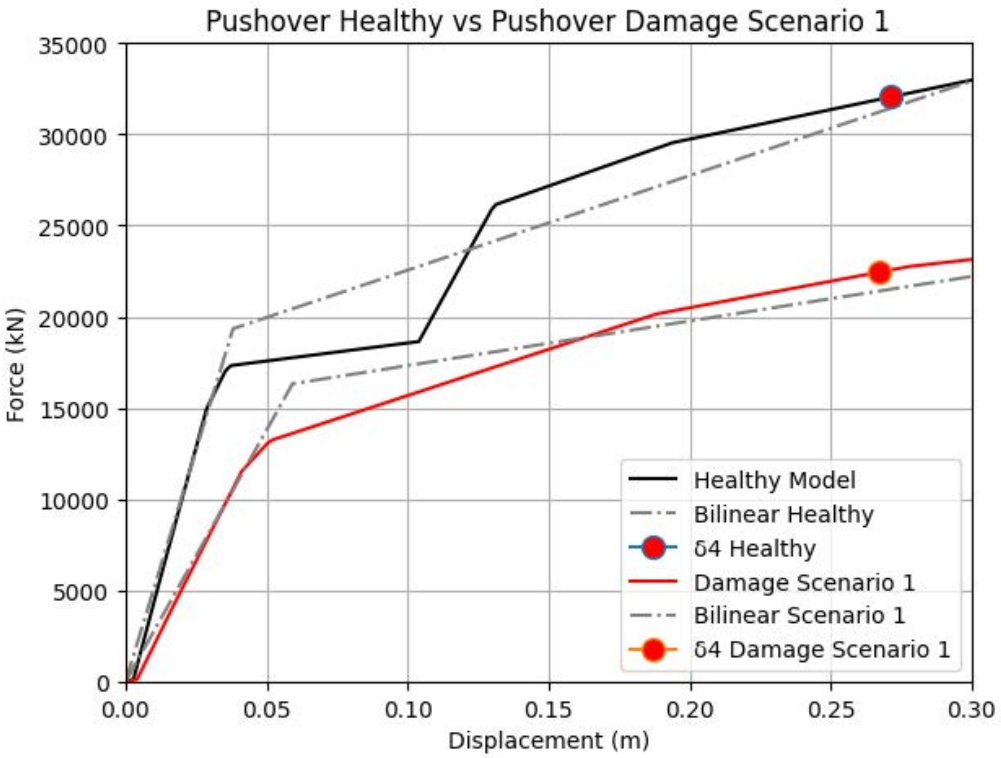

Figure 9. Pushover analysis of undamaged model and damaged model (Scenario 1)

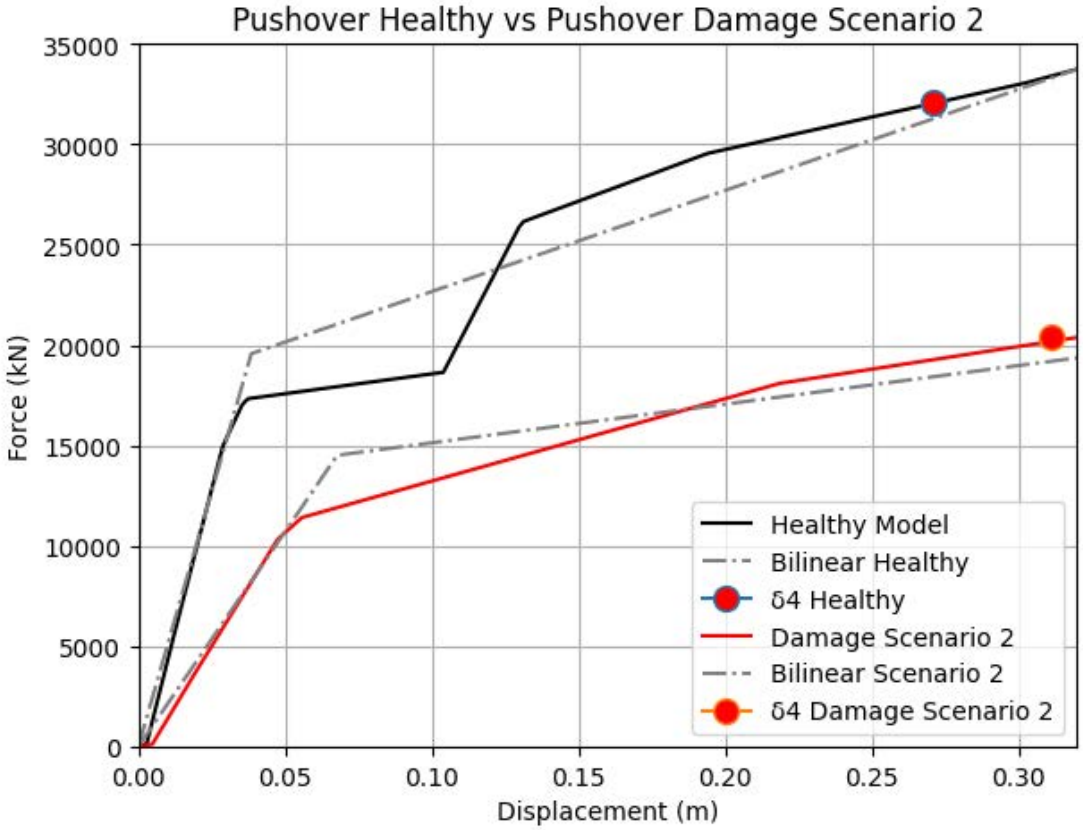

Figure 10. Pushover analysis of undamaged model and damaged model (Scenario 2)

Figure 9 and 10 show the pushover curves of the damaged model of Scenario 1 and Scenario 2, respectively, in comparison to the pushover curve of the undamaged model. By examining the pushover curves of the damaged model, it is evident that its load-carrying capacity has been decreased. Moreover, the comparison of the two pushover curves reveals a significant difference in stiffness, with the damaged model exhibiting a lower stiffness compared to the healthy one. In the healthy model's pushover curve, distinct stiffness changes (change of slope) are observed. The first change in slope occurs at the position corresponding to a lateral force of 17000 kN, coinciding with the occurrence of pier-yielding phenomena. Additionally, a second change in stiffness is observed at a displacement of 0.10 m, indicating the contribution of abutment stiffness after the closure of the gap. Based on an analysis of the pushover curves of the damaged models, notable variations in stiffness are evident. Specifically, a discernible change in stiffness can be observed in the pushover curves of damaged model 1 and damaged model 2. These changes occur at approximately 13000 kN and 12000 kN load magnitudes, respectively. Upon examining the pushover curves of the damaged models, it is evident that the initial slope of these curves reflects the combined stiffness originating from both the abutment and the piers. However, unlike the healthy model pushover curve, the activation mechanism of the abutment is not readily apparent in the damaged models' curves. As the piers yield, a notable alternation in stiffness occurs. Subsequently, the post yield behavior of the structure conforms to the moment-curvature

constitution law assigned to each pier. The aforementioned observations are applicable to both scenarios investigated in this research.

The data points illustrated in Figure 9 and Figure 10 correspond to the displacement at which a 10% reduction in moment occurs within the cross-section constitutive law (hinge) of piers. The displacement ductility (δ_4/δ_y) of each model is $\mu_{\delta,Healthy} = 6.675$, $\mu_{\delta,Damage1} = 4.5166$ $\mu_{\delta,Damage2} = 4.568$. In other words, the healthy model demostrates a higher ductility in comparison to the other two models.

Future investigations can be conducted into models with nonlinearities, such as active and passive damping systems. Examples include models incorporating elastomeric bearings connecting the deck to the piers or employing tuned mass dampers and base isolation techniques for vibration control. The accuracy and precision of the model updating process can be enhanced by applying diverse methodologies. Optimization algorithms like simulated annealing, grey-wolf optimization, colliding bodies optimization, and gravitational search algorithms offer distinct characteristics that can be tailored to meet specific model updating requirements. Furthermore, advanced data-driven methods and machine learning techniques can be explored to enhance damage detection and localization accuracy. Techniques such as artificial neural networks, support vector machines, and ensemble learning methods have shown promise in various structural health monitoring applications, contributing to the refinement of the proposed methodology.

5 AKNOWLEDGEMENTS

The research project was supported by the Hellenic Foundation for Research and Innovation (H.F.R.I.) under the “2nd Call for H.F.R.I. Research Projects to support Faculty Members & Researchers” (Project Number: 4191).

REFERENCES

[1] L. Elfgren, Benchmark of new technologies to extend the life of elderly rail infrastructure: Deliverable D1. 1 of the MAINLINE Project. MAINLINE, 2013.

[2] J. Casas, “Assessment and monitoring of existing bridges to avoid unnecessary strengthening or replacement,” presented at the Bridge Maintenance, Safety, Management and Life-Cycle Optimization: Proceedings of the Fifth International IABMAS Conference, Philadelphia, USA, 11-15 July 2010, CRC Press, 2010, p. 444.

[3]J. R. Casas and A. C. Aparicio, “Structural damage identification from dynamic-test data,” Journal of Structural Engineering, vol. 120, no. 8, pp. 2437–2450, 1994.

[4] R. J. Allemang, “The Modal Assurance Criterion – Twenty Years of Use and Abuse,” SOUND AND VIBRATION, 2003.

[5] X. Q. Zhu and S. S. Law, “Structural Health Monitoring Based on Vehicle-Bridge Interaction: Accomplishments and Challenges,” Advances in Structural Engineering, vol. 18, no. 12, pp. 1999–2015, Dec. 2015, doi: 10.1260/1369-4332.18.12.1999.

[6] K.-C. Chang and C.-W. Kim, “Modal-parameter identification and vibration-based damage detection of a damaged steel truss bridge,” Engineering Structures, vol. 122, pp. 156–173, Sep. 2016, doi: 10.1016/j.engstruct.2016.04.057.

[7] O. S. Salawu and C. Williams, “Bridge Assessment Using Forced-Vibration Testing,” Journal of Structural Engineering, vol. 121, no. 2, pp. 161–173, Feb. 1995, doi: 10.1061/(ASCE)0733-9445(1995)121:2(161).

[8] O. Markogiannaki, A. Arailopoulos, D. Giagopoulos, and C. Papadimitriou, "Vibration-based Damage Localization and Quantification Framework of Large-Scale Truss Structures," Structural Health Monitoring, vol. 22, no. 2, pp. 1376–1398, Mar. 2023, doi: 10.1177/14759217221100443.

[9] H. S. Atamturktur, B. Moaveni, C. Papadimitriou, and T. Schoenherr, Eds., Model Validation and Uncertainty Quantification, Volume 3: Proceedings of the 33rd IMAC, A Conference and Exposition on Structural Dynamics, 2015. in Conference Proceedings of the Society for Experimental Mechanics Series. Cham: Springer International Publishing, 2015. doi: 10.1007/978-3-319-15224-0.

[10] F. McKenna, G. L. Fenves and M. H. Scott (2000). Open System for Earthquake Engineering Simulation. University of California, Berkeley, http://opensees.berkeley.edu.

[11] R. Pinho, C. Casarotti, and S. Antoniou, "A comparison of single-run pushover analysis techniques for seismic assessment of bridges," Earthquake Engineering & Structural Dynamics, vol. 36, no. 10, pp. 1347–1362, 2007, doi: 10.1002/eqe.684.

[12] J. H. Tu et al., "On dynamic mode decomposition: Theory and applications," Journal of Computational Dynamics, vol. 1, no. 2, pp. 391–421, 2014, doi: 10.3934/jcd.2014.1.391.

[13] M. O. Okwu, L. K. Tartibu, M. O. Okwu, and L. K. Tartibu, "Particle swarm optimisation," Metaheuristic Optimization: Nature-Inspired Algorithms Swarm and Computational Intelligence, Theory and Applications, pp. 5–13, 2021.

[14] I. G. Mikes and A. J. Kappos, "Optimization of the seismic response of bridges using variable-width joints," Earthquake Engineering & Structural Dynamics, vol. 52, no. 1, pp. 111–127, Jan. 2023, doi: 10.1002/eqe.3751.

[15] S. P. Stefanidou, A. G. Sextos, A. N. Kotsoglou, N. Lesgidis, and A. J. Kappos, "Soil-structure interaction effects in analysis of seismic fragility of bridges using an intensity-based ground motion selection procedure," Engineering Structures, vol. 151, pp. 366–380, 2017.

[15] M. Zhu, F. McKenna, and M. H. Scott, "OpenSeesPy: Python library for the OpenSees finite element framework," SoftwareX, vol. 7, pp. 6–11, Jan. 2018, doi: 10.1016/j.softx.2017.10.009.

[17] Li Yujian and Xu Liye, "Unweighted Multiple Group Method with Arithmetic Mean," in 2010 IEEE Fifth International Conference on Bio-Inspired Computing: Theories and Applications (BIC-TA), Changsha, China: IEEE, Sep. 2010, pp. 830–834. doi: 10.1109/BICTA.2010.5645232.